The Astrophysical Journal, 760:118 (11pp), 2012 December 1 doi:10.1088/0004-637X/760/2/118


# COHERENT BACKSCATTERING VERIFIED NUMERICALLY FOR A FINITE VOLUME OF SPHERICAL PARTICLES

K. Muinonen[1,5], M. I. Mishchenko[2], J. M. Dlugach[3], E. Zubko[1,6], A. Penttilä[1], and G. Videen[4]
[1] Department of Physics, University of Helsinki, Gustaf Hällströmin katu 2a, FI-00014 U. Helsinki, Finland; karri.muinonen@helsinki.fi, evgenij.zubko@helsinki.fi, antti.i.penttila@helsinki.fi
[2] NASA Goddard Institute for Space Studies, 2880 Broadway, New York, NY 10025, USA; michael.i.mishchenko@nasa.gov
[3] Main Astronomical Observatory, National Academy of Sciences of Ukraine, 27 Zabolotny Street, 03680 Kyiv, Ukraine; dl@mao.kiev.ua
[4] Army Research Laboratory, Adelphi, MD 20783, USA; gorden.videen@gmail.com
*Received 2012 March 4; accepted 2012 September 28; published 2012 November 15*

## ABSTRACT

We consider electromagnetic scattering by a spherical volume sparsely and randomly populated by spherical particles of equal size and optical properties. The far-field scattering matrix of the entire volume is computed using an exact method and an approximate method. The former is a direct computer solver of the Maxwell equations called the superposition *T*-matrix method (STMM). The latter is a solver based on numerical Monte Carlo integration of the ladder and cyclical diagrams appearing in the microphysical theory of radiative transfer and coherent backscattering (RT–CB). The quantitative agreement between the STMM and RT–CB computations provides verification of the RT–CB theory. Prominent backscattering features exhibited by the STMM data cannot be reproduced by keeping only the ladder diagrams of RT. Our results strongly support the CB explanation of opposition brightness and polarization phenomena observed for a class of atmosphereless solar-system objects. Further research is necessary to determine the range of quantitative applicability of the RT–CB theory to densely packed particulate media.

*Key words:* minor planets, asteroids: general – planets and satellites: surfaces – polarization – radiative transfer – scattering

*Online-only material:* color figure

## 1. INTRODUCTION

Regolithic surfaces of atmosphereless solar-system objects are prime examples of complex particulate media of astrophysical relevance. The scattering of electromagnetic waves by such media is controlled by the macroscopic Maxwell equations (MMEs; Stratton 1941), which need to be solved in order to interpret the results of telescopic observations and thereby deduce useful macro- and microphysical information (e.g., Videen et al. 2004; Mishchenko et al. 2010). Unfortunately, direct computer modeling of electromagnetic scattering by such surfaces is still impracticable, and one has to rely on approximate approaches. For the past 125 years, one such approach has been the canonical radiative transfer theory (RT; Lommel 1887; Chandrasekhar 1950). More recently, it has been supplemented by the coherent backscattering mechanism (CB), otherwise known as weak localization of electromagnetic waves (e.g., Watson 1969; Barabanenkov et al. 1991). The RT theory is believed to provide an adequate quantitative description of diffuse multiple scattering of light by many-particle objects, while the inclusion of CB causes several prominent backscattering features in the reflected light.

It has been suggested (Shkuratov 1988, 1989; Muinonen 1989, 1990; Muinonen et al. 1991; Mishchenko 1993; Mishchenko & Dlugach 1993; Hapke et al. 1993; Shkuratov et al. 1994) that the CB effect is likely to have astrophysical importance owing to the fact that atmosphereless solar-system objects exhibit two ubiquitous opposition optical phenomena (Muinonen et al. 2002; Rosenbush et al. 2002; Videen & Kocifaj 2002). One of them is a narrow peak of brightness centered at the exact backscattering direction. The other one is a negative polarization branch at small solar phase angles (the Sun–object–observer angle) which, according to more recent observations (see Rosenbush & Mishchenko 2011 for a review), can be accompanied by an extremely narrow and sharp minimum centered at phase angles approaching zero.

The present study is analogous to an earlier study of the CB phenomenon in scattering systems composed of a small number of scattering objects. In the earlier study, Muinonen (1989) has considered the electromagnetic scattering by two particles that are small compared to the wavelength, with the particles treated as electric dipole scatterers. The second-order ladder and cyclical diagrams have been analytically derived, identifying explicitly the CB interference effects resulting in backscattering enhancement and negative linear polarization in second-order scattering. However, first-order scattering has been seen to predominate over second-order scattering so no CB effects have showed up in the total solution.

These results have been extended to the case of scattering by a particle close to an interface between two optically homogeneous and isotropic media (Lindell et al. 1991; Muinonen et al. 1991; Ermutlu et al. 1995). Lindell et al. (1991) have presented the Exact Image Theory solution (EIT) for scattering of electromagnetic waves by a small object located in the same half-space with the incident radiation. Muinonen et al. (1991) have then concentrated on the backscattering characteristics of that system, unveiling explicitly the CB effects due to the second-order interactions between the material half-space and the particle. Both backscattering enhancement and negative polarization have been verified in the full diffuse solution after ensemble averaging. Ermutlu et al. (1995) have extended the EIT analysis to the case of a buried object: due to the absence

[5] Also at the Finnish Geodetic Institute, FI-02431 Masala, Finland.
[6] Also at the Institute of Astronomy, Kharkov National University, UA-61022 Kharkov, Ukraine.

of cyclical interaction paths, this scattering system gives no rise to CB effects.

The recent derivation of the RT equation and the general equations of the theory of CB directly from the MMEs (Mishchenko et al. 2006; Mishchenko 2011) has clarified their physical origin and conditions of applicability. It is important to recognize that the specific idealized notions of RT and CB can be introduced only upon assuming that the particulate medium is sparsely packed. While this assumption is valid for rarified scattering objects such as clouds in planetary atmospheres, it may become inapplicable to planetary regolith surfaces. Therefore, the interpretation of the opposition phenomena observed for many solar-system objects in terms of CB must be done with extreme caution.

It has been demonstrated recently that direct computer solutions of the MMEs for small densely packed volumes of particulate medium do reproduce qualitatively all opposition features predicted by the low-density theory of CB (Mishchenko et al. 2007, 2009a, 2009b; Dlugach et al. 2011; Lumme & Penttilä 2011). This result provides a strong argument in favor of attributing spectacular opposition phenomena observed for many solar-system objects to the effect of CB. However, the inherent limitation of this type of analysis is that one cannot split the direct solution of the MMEs into the RT and CB parts. Therefore, the definitive proof of the CB origin of the opposition features exhibited by the direct solutions of the MMEs is still missing.

The only unequivocal way to establish the physical origin of the opposition features seen in the computer solutions of the MMEs is to perform a quantitative comparison of these solutions with calculations based on the low-density theories of RT and CB. Indeed, in this case the summation of the ladder diagrams describing diffuse multiple scattering of light is separated from the summation of the cyclical diagrams causing CB. What has been missing is direct verification of the RT–CB model using exact MME results.

The availability of the advanced Monte Carlo solver of the RT and CB equations (Muinonen 2004; Muinonen et al. 2010; Muinonen & Videen 2012) as well as of the efficient superposition $T$-matrix solver of the MMEs (Mackowski & Mishchenko 1996, 2011) provides a unique opportunity to address this unresolved yet fundamentally important problem. In this paper, we advance the approach outlined briefly by Muinonen & Zubko (2010) and perform a representative comparison of asymptotically exact MME results and approximate RT–CB computations. This comparison allows us to achieve critical objectives: (1) validate the specific concepts used in the derivation of the RT and CB theories from the MMEs, (2) verify whether specific features exhibited by the solutions of the MMEs can indeed be attributed to the effect of CB, and (3) examine how stringent are the restrictions of the RT–CB theory.

## 2. SCATTERING THEORY

### 2.1. General Methodology

We use the model of a random particulate medium in the form of an imaginary spherical volume of radius $R$ fully enclosing $N$ identical non-overlapping spherical particles of radius $r$ (see Figure 1). The size parameter of the volume is $kR$, while the particle size parameter is $kr$, where $k$ is the wave number in the homogeneous and nonabsorbing host medium. All particles populating a scattering volume have the same relative refractive index $m$. The distribution of particle positions

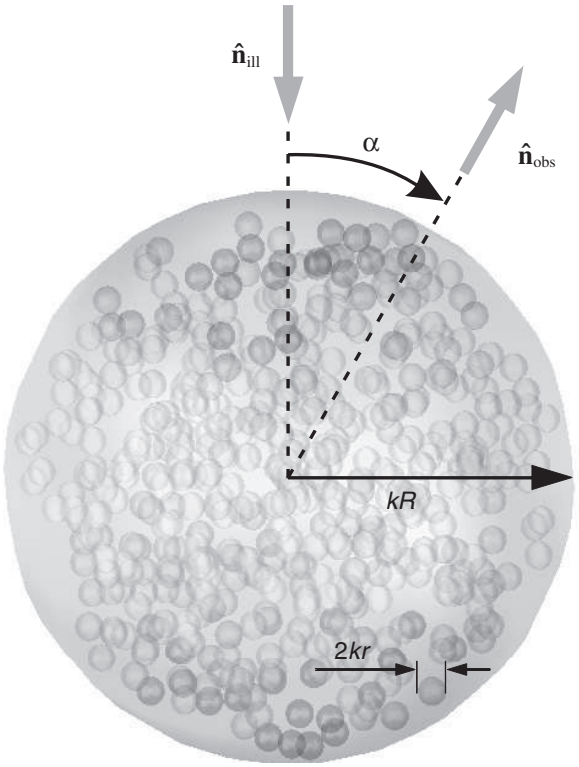


**Figure 1.** Scattering by a spherical volume randomly filled with small spherical particles.

throughout the volume is assumed to be totally random and statistically uniform.

It is assumed that the particulate volume is illuminated by a parallel quasi-monochromatic beam of light propagating in the direction of the unit vector $\hat{\boldsymbol{n}}_{\rm ill}$ (Figure 1). The observer is located in the far-field zone of the entire spherical volume in the scattering direction specified by the unit vector $\hat{\boldsymbol{n}}_{\rm obs}$. Owing to statistical randomness of particle positions, the ensemble-averaged scattering and absorption properties of the particulate volume depend only on the phase angle $\alpha$ (i.e., the angle between the vectors $\hat{\boldsymbol{n}}_{\rm obs}$ and $-\hat{\boldsymbol{n}}_{\rm ill}$) provided that the scattering plane is used for defining the Stokes parameters of the incident and scattered light. The far-field transformation of the Stokes parameters $I$, $Q$, $U$, and $V$ upon scattering by the entire particulate volume is then formulated in terms of the $4 \times 4$ real-valued scattering matrix (e.g., Mishchenko et al. 2006)

$$\begin{bmatrix} I^{\rm sca} \\ Q^{\rm sca} \\ U^{\rm sca} \\ V^{\rm sca} \end{bmatrix} \propto \begin{bmatrix} P_{11} & P_{21} & 0 & 0 \\ P_{21} & P_{22} & 0 & 0 \\ 0 & 0 & P_{33} & P_{34} \\ 0 & 0 & -P_{34} & P_{44} \end{bmatrix} \begin{bmatrix} I^{\rm inc} \\ Q^{\rm inc} \\ U^{\rm inc} \\ V^{\rm inc} \end{bmatrix}, \qquad (1)$$

where the superscripts "inc" and "sca" stand for "incident" and "scattered", respectively.

The elements of the scattering matrix can be used to define conventional optical observables corresponding to different types of polarization state of the incident radiation used in remote-sensing, in situ, and laboratory particle characterization. Specifically, if the incident light is unpolarized then the phase function $P_{11}$ characterizes the angular distribution of the far-field scattered intensity, while the ratio $P = -P_{21}/P_{11}$ gives the corresponding degree of linear polarization. If the incident radiation is polarized linearly in the scattering plane (i.e., $Q^{\rm inc} = I^{\rm inc}$, $U^{\rm inc} = V^{\rm inc} = 0$) then the linear polarization ratio

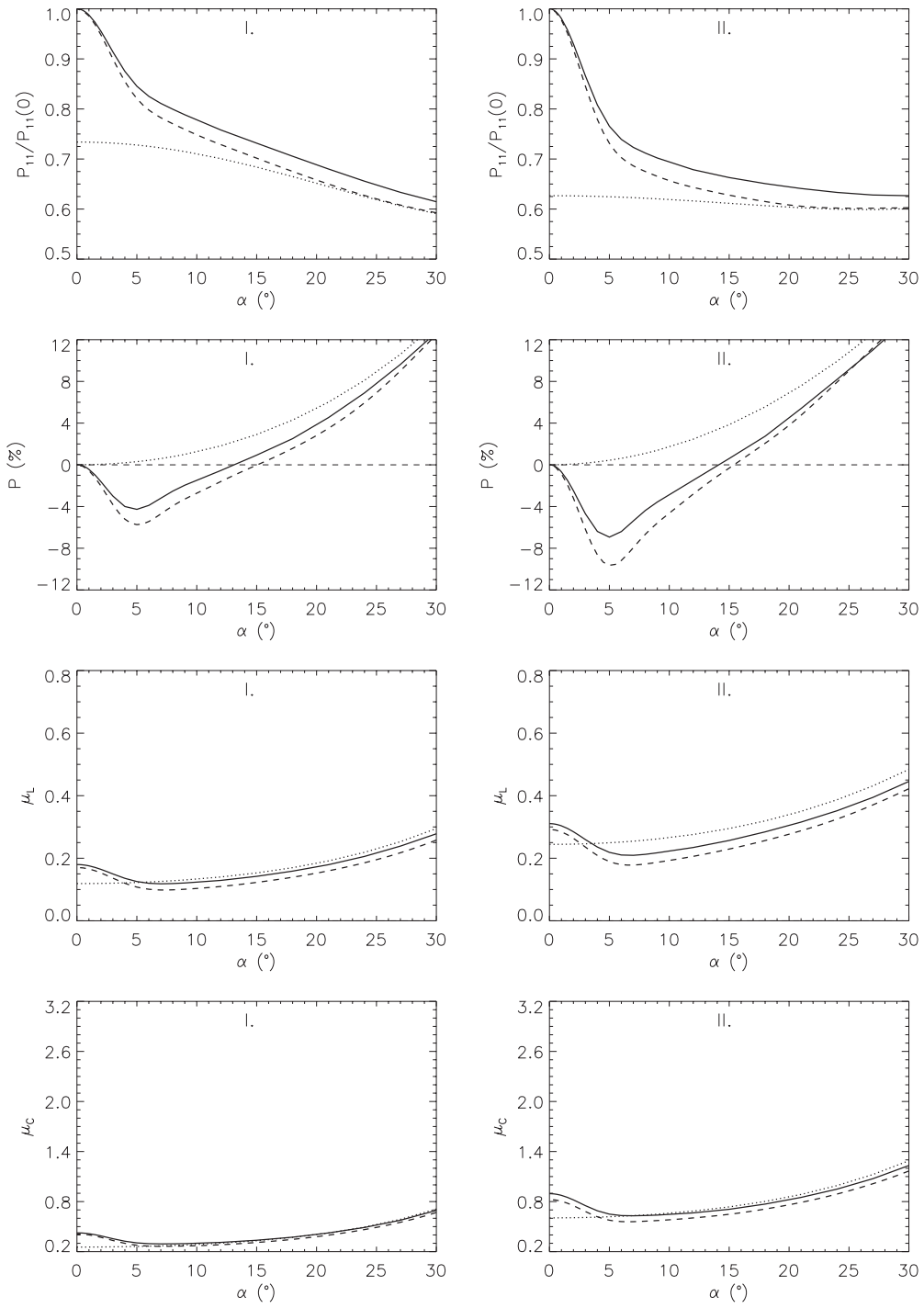


**Figure 2.** Scattering by a spherical volume of particulate medium with a size parameter $kR = 40$ and packing density of $v = 3.125\%$ (I) and 6.250% (II), populated with spherical particles with a size parameter $kr = 2$ and a refractive index $m = 1.31$. The solid, dotted, and dashed curves depict the RT–CB, RT-only, and STMM results, respectively. See the text.

$\mu_L$ is defined as the ratio of the cross-polarized and co-polarized components of the scattered intensity:

$$\mu_L = \frac{P_{11} - P_{22}}{P_{11} + 2P_{21} + P_{22}}. \quad (2)$$

If the incident radiation is polarized circularly in the counterclockwise direction when looking in the direction of propagation (i.e., $V^{inc} = I^{inc}$, $Q^{inc} = U^{inc} = 0$), then the circular polarization ratio $\mu_C$ is defined as the ratio of the same-helicity and opposite-helicity components of the scattered intensity:

$$\mu_C = \frac{P_{11} + P_{44}}{P_{11} - P_{44}}. \quad (3)$$

### 2.2. Radiative Transfer with Coherent Backscattering

The RT–CB method is based on the Monte Carlo integration of the ladder and cyclical diagrams (Muinonen 2004), wherein CB is computed alongside RT by incorporating the reciprocity relation in electromagnetic scattering (Saxon 1955) and keeping

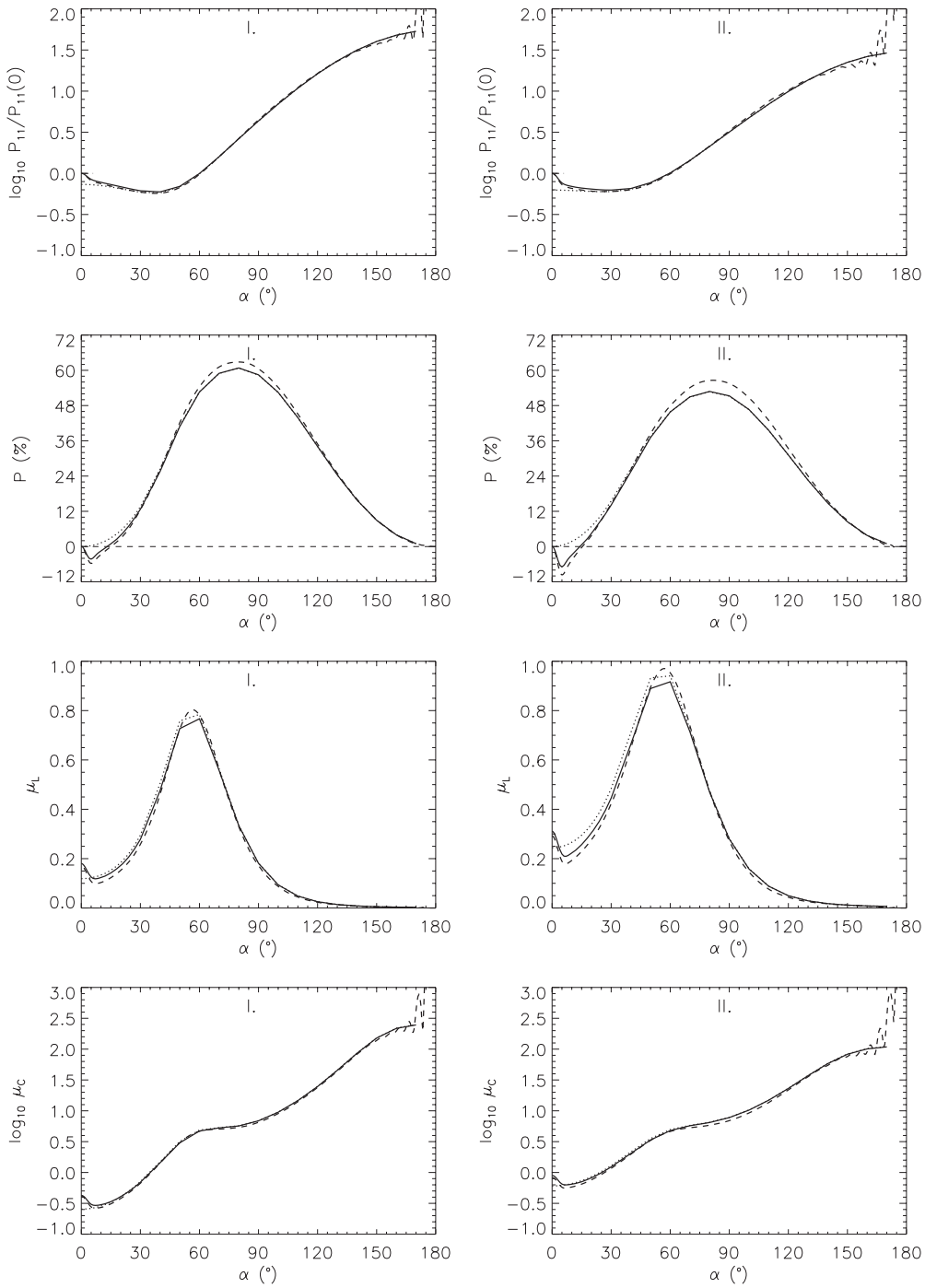


**Figure 3.** Same as in Figure 2, but for the full range of phase angles.

the relative phase information of the wave components. The notion of the ladder and cyclical diagrams is explained briefly in the Appendix. In the original work, the RT–CB method has been presented for a plane-parallel medium of particles; subsequently, it has been customized for a spherical particulate medium (Muinonen et al. 2010).

More recently, the RT–CB method has been further modified so that it makes use of scattering-amplitude matrices in the computation of the ladder and cyclical diagrams, allowing for the reciprocity relation to be utilized in monitoring the accuracy of the numerical computation (Muinonen & Videen 2012). Furthermore, the incorporation of symmetries into the wave propagation with different polarization states has resulted in improved convergence of the Monte Carlo integration near the backscattering direction.

### 2.3. Superposition T-matrix Method

The superposition *T*-matrix method (STMM; Mackowski & Mishchenko 1996, 2011) is a direct computer solver of the MMEs for a fixed multi-sphere group. Within the range of its numerical convergence, the corresponding public-domain STMM computer code yields results with a guaranteed accuracy, which makes it numerically exact.

To model statistically random and uniform particle positions within the spherical volume consistent with the fundamental

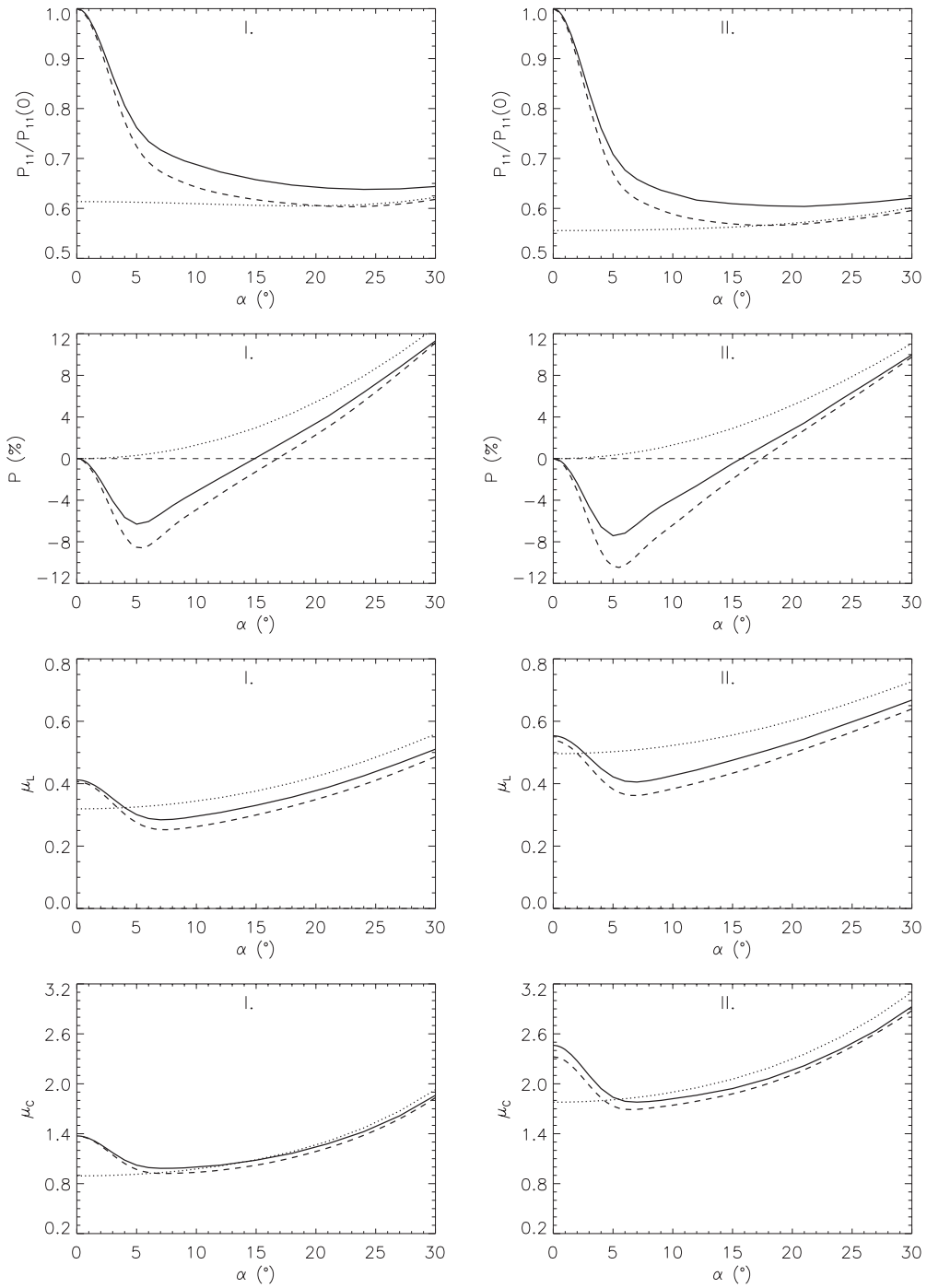


**Figure 4.** Same as in Figure 2, but for $kr = 1.76$, $m = 1.50$, and $v = 2.130\%$ (I) or 4.259% (II).

assumption of ergodicity, we follow the approach by Mishchenko et al. (2007). Specifically, we create a realization of an $N$-sphere group generated randomly according to the procedure described by Mackowski (2006) and then average the elements of the scattering matrix over the uniform orientation distribution of this configuration with respect to the laboratory coordinate system. Although the mutual positions of the $N$ particles with respect to each other remain fixed, they are quite random from the outset. Therefore, this straightforward approach yields, in effect, an infinite continuous set of random realizations of the scattering volume while enabling us to use the highly efficient orientation averaging procedure afforded by the analyticity of the STMM formulation.

An essential feature of the analytical orientation averaging procedure is that it generates results that are completely free of noise potentially caused by the discreteness of orientations used in the numerical averaging procedure (cf. Voit et al. 2009; Penttilä & Lumme 2011). This feature ensures definitive identification of subtle optical effects and their correct attribution. To re-enforce the statistical randomness of a scattering particulate volume, each STMM result shown below has been obtained by averaging over five independently generated $N$-sphere configurations. Such averaging has been found to be adequate for the present comparison through gradual increase of the number of sample volumes. It is inevitable, however, that a certain amount of numerical noise always

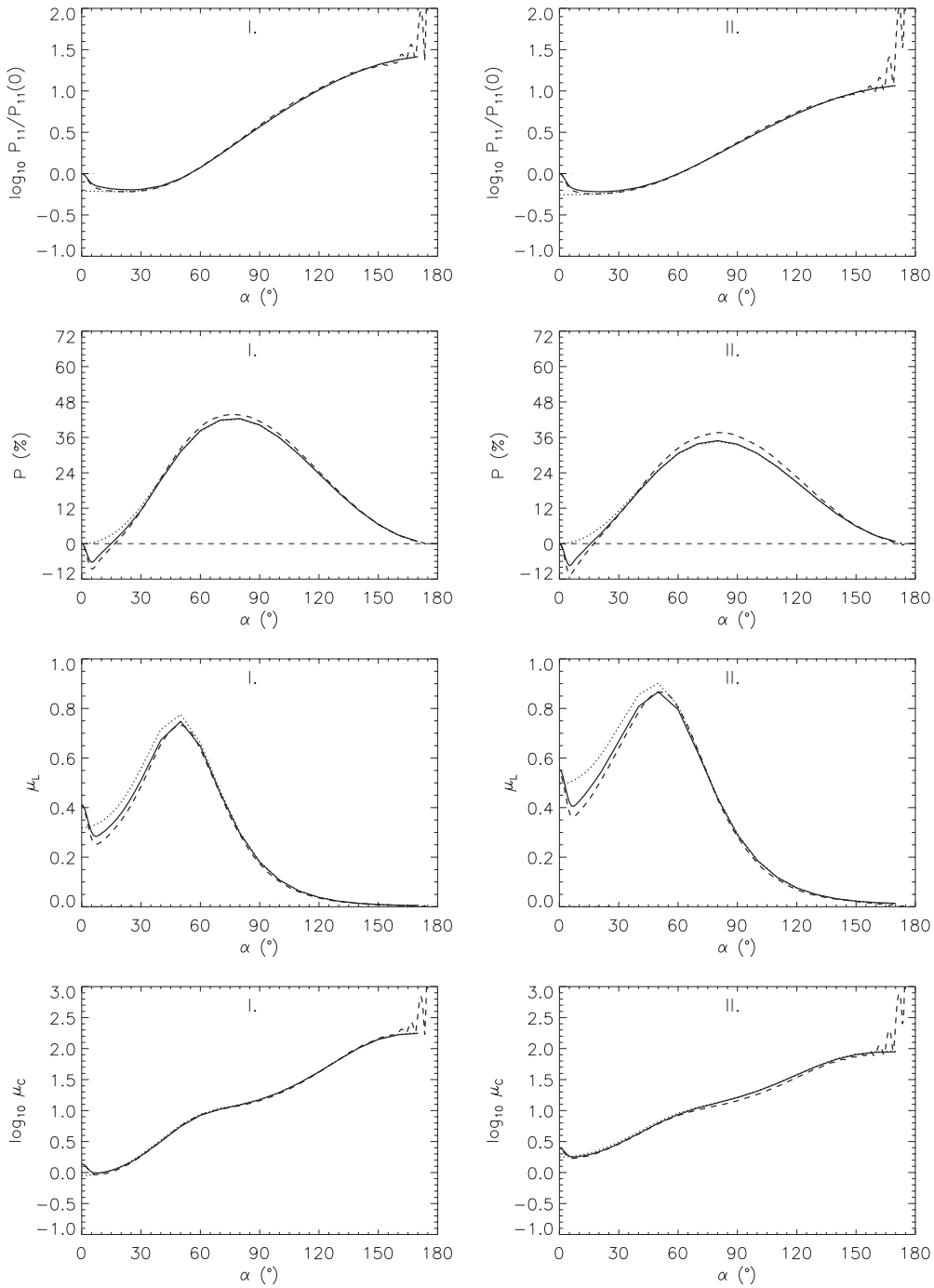


**Figure 5.** Same as in Figure 4, but for the full range of phase angles.

remains due to averaging using a finite number of sample volumes.

## 3. NUMERICAL RESULTS AND DISCUSSION

RT–CB and STMM computations have been carried out for specific finite random media of spherical particles with $kR = 40$. First, for the monomer refractive index $m = 1.31$ and size parameter $kr = 2$, the numbers of constituent spheres $N$ (STMM) and the corresponding packing densities (RT–CB) have been $N = 250$, $v = 3.125\%$ and $N = 500$, $v = 6.25\%$, where the packing density is defined as $v = Nr^3/R^3$. Second, for $m = 1.50$ and $kr = 1.76$, the particle numbers $N = 250$ and $N = 500$ have implied packing densities $v = 2.130\%$ and $4.259\%$. The Monte Carlo RT–CB computations with 100,000 rays have required several hours of computing time on a single processor per each of the four cases.

Figures 2–5 show separately the RT–CB and RT-only results for the scattering phase function, the degree of linear polarization for incident unpolarized light, and for the linear and circular polarization ratios, all as functions of the phase angle. Also shown are the ensemble-averaged STMM results.

It must be recognized that the RT–CB theory is fundamentally based on the asymptotic requirements $v \ll 1$ and $N \gg 1$ (Mishchenko et al. 2006). The former inequality ensures that each particle is located in the far-field zones of all the other particles populating the medium and also is a necessary condition

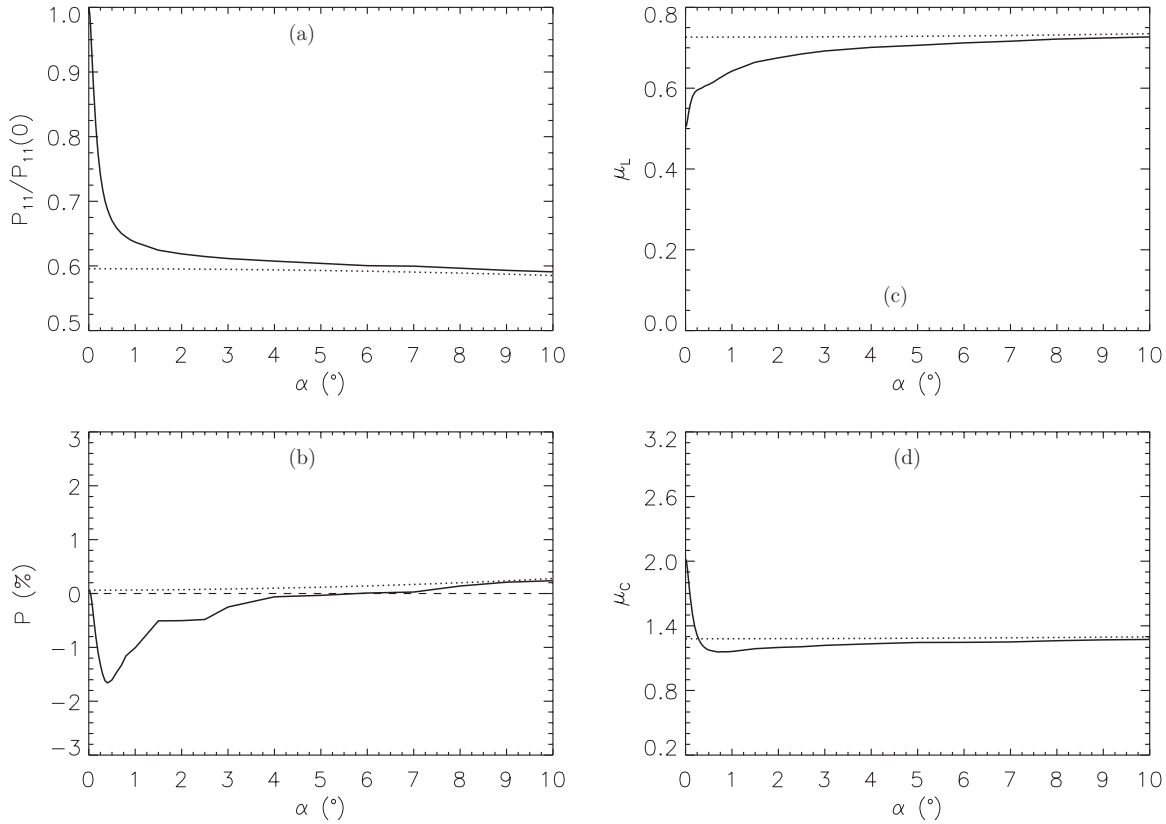


**Figure 6.** RT–CB (solid lines) and RT-only computations (dotted lines) for a macroscopic medium with $kR = 10^7$ composed of a power-law size distribution (index $v = 3$) of spherical monomers with sizes within $kr \in [2.0, 3.0]$. The refractive index of the monomers is $m = 1.31 + i10^{-3}$ and the volume density is $v = 3.125\%$. (a) $P_{11}/P_{11}(0)$, (b) $P = -P_{21}/P_{11}$, (c) $\mu_L = (P_{11} - P_{22})/(P_{11} + 2P_{21} + P_{22})$, and (d) $\mu_C = (P_{11} + P_{44})/(P_{11} - P_{44})$.

for assuming that particle positions inside the volume are totally random and mutually independent. The latter inequality allows one to ignore looped (i.e., non-self-avoiding) diagrams in the far-field order-of-scattering expansion of the electromagnetic field. The combination of these limits implies that $kR \gg 1$.

While these inequalities are essential in the derivation of the RT–CB theory from the MMEs (Mishchenko et al. 2006), this derivation does not yield specific numerical estimates of the largest allowable packing density and the smallest allowable number of particles. Such estimates can only be derived from quantitative comparisons of the approximate RT–CB results and numerical data obtained by directly solving the MMEs.

These well-established facts along with the numerical data displayed in Figures 2– 5 imply the following important and instructive results.

1. Although the random particulate volumes studied contain modest numbers of particles, the packing density deviates from zero significantly, and the size parameter of the volumes is moderate, the quantitative agreement between the STMM and approximate RT–CB results is quite evident.
2. The only phase-angle range where the STMM and RT—CB results disagree is that corresponding to forward-scattering directions. This result is predictable and is explained by different ways of treating the effect of forward-scattering interference (Mishchenko et al. 2007; Muinonen 1989). Indeed, in the framework of the approximate microphysical RT–CB theory, this effect is incorporated mathematically in the computation of the exponential attenuation rate inside the volume (Mishchenko et al. 2006), whereas, in the framework of the far-field STMM computations it causes the strong and exceedingly narrow diffraction peak.
3. Outside a relatively narrow range of backscattering geometries, the full RT–CB and the RT-only results are very similar. This result is consistent with the physical interpretation of CB as a backscattering interference mechanism.
4. The RT-only results cannot reproduce the backscattering peaks in $P_{11}$, $\mu_L$, and $\mu_C$ as well as the asymmetric polarization minimum at small phase angles exhibited by the STMM results. The inclusion of the cyclical diagrams allows us to reproduce these backscattering features very closely, which provides a definitive proof of their CB nature.
5. In all the cases considered, the effect of CB is noticeable to phase angles exceeding 20°. Furthermore, the angular widths of the CB phenomena are rather insensitive to packing density. Both traits can be explained by the modest size parameter of the particulate volumes and the moderately forward-scattering tendency of the constituent spheres. As a consequence, $kR$ rather than the transport mean free path defines the mean length of the interference base and thus the angular width of the backscattering features (cf. Barabanenkov et al. 1991; Mishchenko et al. 2009a, 2009b).
6. The origin of the small residual differences between the STMM and RT–CB results at side- and backscattering angles remains uncertain. These differences do seem to decrease with decreasing packing density, which would be an expected result. However, they still persist even for packing densities as small as 2.130%, probably because the reduction of $v$ is achieved by decreasing the number of constituent particles and thus violating more significantly

the requisite inequality $N \gg 1$. These observations call for additional computations in which $v$ is reduced while $N$ is kept constant.

To further demonstrate the astrophysical relevance of our methodology, the RT–CB method is applied to compute the backscattering characteristics of a spherical medium with macroscopic size $kR = 10^7$ (i.e., for $\lambda = 2\pi/10\,\mu$m, $R = 1.0$ m) composed of a size distribution of absorbing spherical monomers with $m = 1.31 + i10^{-3}$. The size parameter varies from $kr = 2$ to $kr = 3$ according to a power-law size distribution with index $\nu = 3$ (see Muinonen et al. 2010). Altogether 11 different monomer sizes are utilized ($kr = 2.0, 2.1, 2.2, \ldots, 3.0$) and the volume density is $v = 3.125\%$. The average single-scattering albedo takes a high value of $\tilde{\omega} = 0.99112$ and the extinction mean free path converted to the size parameter range is $k\ell = 100.31$. The computations have been carried out utilizing 160,000 rays and have taken more than four days of computing time on an eight-core computer.

The Bond and geometric albedos of the spherical medium turn out to be $A = 0.67$ and $p = 0.65$, respectively, values not atypical of high-albedo atmosphereless solar-system objects. Figure 6 shows the backscattering enhancement and degree of linear polarization for the spherical medium. As the narrow size distribution neutralizes the polarization in average single scattering, the resulting negative polarization from coherent backscattering is also weakened. In absolute terms, the polarization peaks at roughly $-1.7\%$ at a phase angle of $0\overset{\circ}{.}4$; that is, the polarization becomes comparable to what has been observed for certain atmosphereless solar-system objects (Boehnhardt et al. 2004; Rosenbush and Mishchenko 2011). The backscattering peak is narrow with an enhancement factor of 1.68 over the RT-only background.

Comparing Figure 6 with Figures 2–5, the angular dependences are drastically sharper for the dependences of the macroscopic medium. In comparison to case I in Figure 2 with an equal volume density of $v = 3.125\%$, on one hand, there is a complete reversal of $\mu_{\rm L}$ near backscattering: for the macroscopic medium, $\mu_{\rm L}$ shows a narrow and prominent downward surge, whereas a wide and moderate upward surge is evident for the microscopic medium. For $\mu_{\rm C}$, on the other hand, the upward surge is further strengthened for the macroscopic medium. These results compare favorably with the computations by Muinonen (2004) for optically thick plane-parallel media of spherical particles with varying absorption as well as with the experimental measurements of linear and circular polarization ratios for lunar samples by Hapke et al. (1993). Our computations corroborate the result by Mishchenko & Liu (2009) that CB can cause a backscattering enhancement in $\mu_{\rm L}$ for optically thin particulate media that gradually evolves into a backscattering depression for optically thick media.

## 4. CONCLUSIONS

In summary, first, the quantitative agreement between the STMM and RT–CB results obtained with full account of polarization provides the first direct and definitive corroboration of the microphysical RT–CB approach (Mishchenko et al. 2006). We have verified in previous studies that the prominent backscattering features exhibited by the STMM data cannot be reproduced by accounting for only the ladder diagrams of RT. Thus, second, our results strongly support the CB explanation of the spectacular opposition optical phenomena observed for many atmosphereless solar-system objects. Perhaps of most practical significance is that our results suggest that, to an extent, the stringent restrictions of the RT model regarding particle packing density can be relaxed. Satisfactory results can be obtained using the RT–CB model for relatively dense media.

From an astrophysical perspective, it should be recognized that our numerically exact STMM data are obtained for a rather simple model of a particulate medium. It is, therefore, not surprising that the amplitude of the brightness opposition effect and the depth of the negative polarization minimum in Figures 2 and 4 exceed those observed, for example, for high-albedo satellites of Jupiter and Saturn as well as for E-type asteroids (Rosenbush and Mishchenko 2011). Indeed, it is unlikely that the entire surfaces of these objects are covered by the same microscopic grains causing uniformly the same opposition effects via the CB effect. The angular widths of the observed effects are also predictably smaller than those in Figures 2 and 4. The interference base for a finite scattering volume is controlled by its size parameter $kR$, whereas that for an optically thick, nonabsorbing, or weakly absorbing regolith layer is controlled by the product $k\ell_{\rm tr}$ of the wave number and the transport mean free path (Barabanenkov et al. 1991). The actual values of $k\ell_{\rm tr}$ for bright solar-system objects are likely to be much greater than the $kR$ values used in our computations and result in much narrower opposition effects. Figure 6 shows the first evidence of such neutralization of polarization and narrowing of the angular widths.

It should be recognized, however, that the photometric and polarimetric observations for several high-albedo atmosphereless solar-system objects (Rosenbush and Mishchenko 2011) are unique in that they reveal coexisting brightness and polarization effects of comparable angular widths and with angular profiles consistent with the numerically exact STMM computations. So far, no other first-principles theory of electromagnetic scattering has been able to reproduce both effects with their very specific traits simultaneously. Therefore, the results of our comparisons of the STMM and CB computations strongly point to the CB origin of the observed opposition phenomena. It is expected that the much greater flexibility of the RT–CB theory (in terms of the size and composition of a particulate medium) and its potential applicability to regolith surfaces with realistic packing densities will eventually result in significantly better fits of theoretical computations to observational results (cf. Figure 6).

There is an extensive amount of future work needed to determine the range of quantitative applicability of the RT–CB theory in terms of particle packing density and particulate medium size. The success of the RT–CB theory applied to finite media of particles calls for a parallel treatment of electromagnetic scattering by large compact particles. In this spirit, initial studies have been carried out for the so-called exploding particle by Zubko et al. (2008) with the use of the discrete-dipole approximation. This technique can be applied, in particular, to the study of the role of the so-called near fields in scattering by aggregates where the constituent particles are in contact with one another.

This research has been partially funded by the Academy of Finland (contract 127461), NASA Outer Planets Research Program (contract NNX10AP93G), and NASA Lunar Advanced Science and Exploration Research Program (contract NNX11AB25G), as well as by the NASA Radiation Sciences Program managed by Hal Maring and by the NASA Remote Sensing Theory Program managed by Lucia Tsaoussi. M.I.M. and J.M.D. also acknowledge support from the National

Academy of Sciences of Ukraine under the Main Astronomical Observatory GRAPE/GPU/GRID Computing Cluster Project.

## APPENDIX

## LADDER AND CYCLICAL DIAGRAMS

The concept of ladder and cyclical diagrams is most conveniently introduced in the framework of the so-called Foldy–Lax equations (FLEs) which are mathematically equivalent to the MMEs and describe electromagnetic scattering by an arbitrary group of $N$ discrete particles (Mishchenko et al. 2006). The FLEs allow one to decompose the total electric, $\boldsymbol{E}$, and magnetic, $\boldsymbol{H}$, fields at an observation point $\boldsymbol{r}$ into the respective incident fields and individual-particle contributions:

$$\boldsymbol{E}(\boldsymbol{r}) = \boldsymbol{E}^{\rm inc}(\boldsymbol{r}) + \sum_{i=1}^{N} \boldsymbol{E}_i(\boldsymbol{r}),$$

$$\boldsymbol{H}(\boldsymbol{r}) = \boldsymbol{H}^{\rm inc}(\boldsymbol{r}) + \sum_{i=1}^{N} \boldsymbol{H}_i(\boldsymbol{r}). \tag{A1}$$

Each $i$th partial field can, in turn, be represented mathematically as a superposition of contributions from all possible particle sequences ending at particle $i$:

$$\boldsymbol{E}_i(\boldsymbol{r}) = \boldsymbol{E}_{i0}(\boldsymbol{r}) + \sum_{j=1,j\neq i}^{N} \boldsymbol{E}_{ij}(\boldsymbol{r}) + \sum_{j=1,j\neq i}^{N} \sum_{k=1,k\neq j}^{N} \boldsymbol{E}_{ijk}(\boldsymbol{r}) + \cdots, \tag{A2}$$

where $\boldsymbol{E}_{i0}(\boldsymbol{r})$ is the direct response of particle $i$ to the incident field, and similarly for $\boldsymbol{H}_i(\boldsymbol{r})$. Examples of such multiple-scattering sequences are shown in Figure 7(a). Combining Equations (A1) and (A2) results in

$$\boldsymbol{E}(\boldsymbol{r}) = \boldsymbol{E}^{\rm inc}(\boldsymbol{r}) + \sum_{i=1}^{N} \boldsymbol{E}_{i0}(\boldsymbol{r}) + \sum_{i=1}^{N} \sum_{j=1,j\neq i}^{N} \boldsymbol{E}_{ij}(\boldsymbol{r}) + \sum_{i=1}^{N} \sum_{j=1,j\neq i}^{N} \sum_{k=1,k\neq j}^{N} \boldsymbol{E}_{ijk}(\boldsymbol{r}) + \cdots, \tag{A3}$$

and an analogous formula follows for $\boldsymbol{H}(\boldsymbol{r})$.

In general, the explicit analytical expressions for the individual terms in the decomposition (A3) are quite complex. They can, however, be drastically simplified upon making the following two assumptions.

1. The $N$ particles forming the group are separated widely enough that each of them is located in the far zones of all the other particles.
2. The observation point is located in the far zone of any particle forming the group.

Both assumptions imply that the particulate medium in question is sparsely packed.

Thus, the order-of-scattering expansion (A3) and its magnetic counterpart allow one to represent the total field at a point in space as a sum of contributions arising from all possible particle sequences. The next major assumption, called the Twersky approximation, is that all sequences involving a particle more than once can be neglected. For example, the self-avoiding sequences (i)–(iii) in Figure 7(a) are kept, whereas the sequence (iv) is excluded. It can be proven that the Twersky approximation is justified provided that the number of particles in the scattering volume is very large. Thus, instead of Equation (A3), we have

$$\boldsymbol{E}(\boldsymbol{r}) = \boldsymbol{E}^{\rm inc}(\boldsymbol{r}) + \sum_{i=1}^{N} \boldsymbol{E}_{i0}(\boldsymbol{r}) + \sum_{i=1}^{N} \sum_{j=1,j\neq i}^{N} \boldsymbol{E}_{ij}(\boldsymbol{r}) + \sum_{i=1}^{N} \sum_{j=1,j\neq i}^{N} \sum_{k=1,k\neq i,k\neq j}^{N} \boldsymbol{E}_{ijk}(\boldsymbol{r}) + \cdots, \tag{A4}$$

and similarly for $\boldsymbol{H}(\boldsymbol{r})$. Note that the very applicability of the Twersky approximation makes the limit $N \rightarrow \infty$ an explicit assumption in the solution of the electromagnetic scattering problem.

The Stokes parameters in the far zone of the entire $N$-particle group can be found from the configuration-averaged so-called Poynting–Stokes tensor $\langle \boldsymbol{H} \otimes \boldsymbol{E} \rangle$ (Mishchenko 2011), where $\otimes$ denotes dyadic multiplication of two vectors. Obviously, the computation of $\langle \boldsymbol{H} \otimes \boldsymbol{E} \rangle$ requires ensemble averaging of the dyadic products of the type $\boldsymbol{H}_{i\ldots k} \otimes \boldsymbol{E}^*_{l\ldots m}$. Each such product can be depicted diagrammatically as exemplified in Figure 7(b), in which the magnetic-field term $\boldsymbol{H}_{4321}$ is represented by blue arrows, while the electric-field term $\boldsymbol{E}^*_{765}$ is depicted by yellow arrows.

The very essence of the ladder approximation is to keep only a certain class of diagrams. The simplest ladder diagram is shown in Figure 7(c) and corresponds to the product $\boldsymbol{H}_{n,n-1,\ldots,2,1} \otimes \boldsymbol{E}^*_{n,n-1,\ldots,2,1}$ In other words, all $n$ particles are common to the corresponding magnetic- and electric-field terms and appear in exactly the same order. Figure 7(d) shows a more complicated ladder diagram in which the same $n$ particles are common to both terms and appear in the same order. However, the magnetic-field sequence contains an additional uncommon particle, while the electric-field sequence contains two uncommon particles. Obviously, this diagram corresponds to the product $\boldsymbol{H}_{n,l,n-1,\ldots,2,1} \otimes \boldsymbol{E}^*_{n,n-1,\ldots,2,i,j,1}$. Thus, the main characteristic of the ladder diagrams is that all common particles appear in corresponding magnetic- and electric-field sequences in exactly the same order.

The main justification for using the ladder approximation is that averaging over random positions of participating particles can be expected to extinguish the contribution of any multi-particle diagram with no common particles appearing in the same order, like, e.g., the diagram shown in Figure 7(b). Indeed, the result of interference of the two waves in Figure 7(b) at the observation point fluctuates randomly as the particles move and eventually averages out. On the other hand, the phase difference between the two waves in Figure 7(c) is identically equal to zero, while averaging over all positions of all uncommon particles (such as particles $i$, $j$, and $l$ in Figure 7(d)) results in the standard exponential attenuation law.

Although analytical summation of all ladder diagrams is still a mathematically involved procedure, the final result is the integral form of the well-known vector RT equation for the specific Stokes column vector (Mishchenko et al. 2006). There are many numerical techniques that can be used to solve the RT equation. However, the Monte Carlo method used in our calculations is particularly flexible and can easily be applied to a spherical volume of particulate medium such as that shown in Figure 1.

Thus the microphysical derivation of the RT equation from the MMEs explicitly ignores the contribution of so-called cyclical diagrams exemplified by Figures 7(e) and (f). In this case

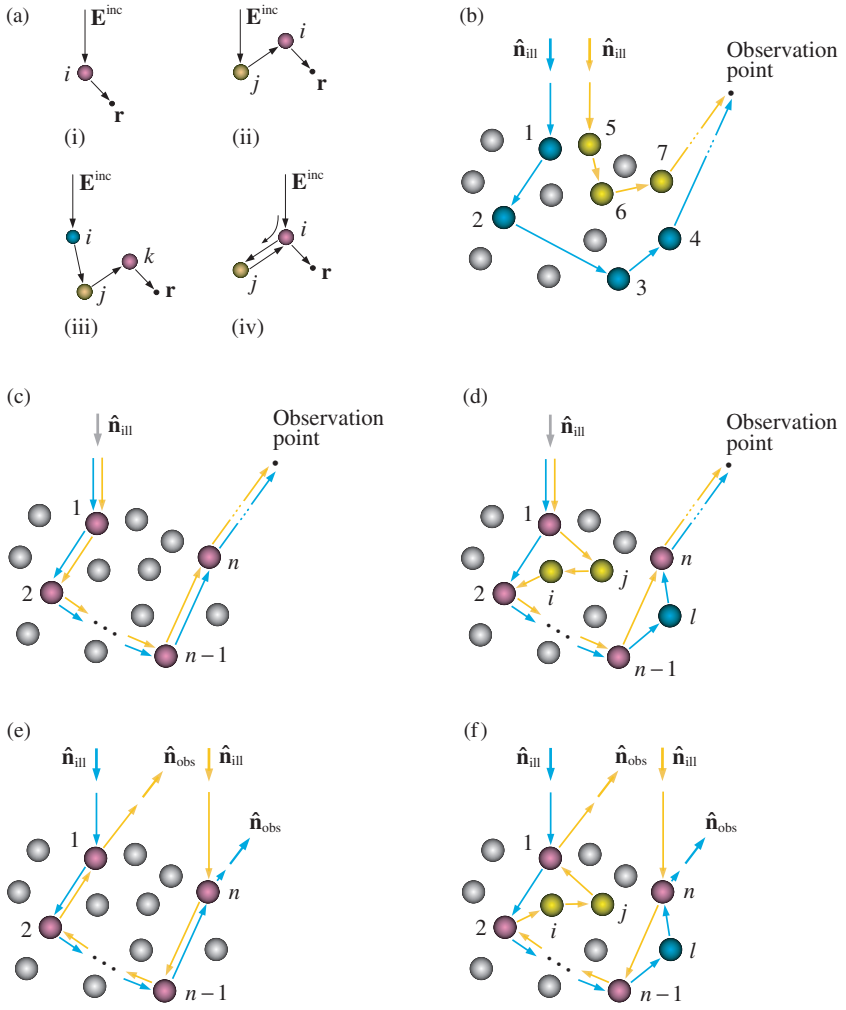


**Figure 7.** (a) Examples of multi-particle sequences contributing to Equation (A3). (b) Diagrams contributing to the Poynting–Stokes tensor of the total field. (c, d) Ladder diagrams. (e, f) Cyclical diagrams.

(A color version of this figure is available in the online journal.)

particles $1, 2, \ldots, n-1, n$ are common to a pair of multi-particle sequences but appear in the reverse order (cf. Figures 7(e) and (c) and Figures 7(f) and (d)). The cyclical diagrams composed of such conjugate multi-particle sequences usually provide a negligible contribution to the scattered intensity, but cause a significant CB effect in the immediate vicinity of the exact backscattering direction ($\hat{\boldsymbol{n}}_{\rm obs} = -\hat{\boldsymbol{n}}_{\rm ill}$). Indeed, there the phase difference between any conjugate multi-particle paths vanishes, thereby causing consistently constructive interference and a pronounced CB peak in intensity. Importantly, averaging over all positions of all uncommon particles (such as particles $i$, $j$, and $l$ in Figure 7(f)) again results in the exponential attenuation law.

Numerical summation of all the cyclical diagrams is more involved than the solution of the vector RT equation. It requires a modification of the standard Monte Carlo solver wherein the wave-phase information is carefully preserved and accounted for (Muinonen 2004).

## REFERENCES


Barabanenkov, Yu. N., Kravtsov, Yu. A., Ozrin, V. D., & Saichev, A. 1991, Prog. Opt., 29, 65

Boehnhardt, H., Bagnulo, S., Muinonen, K., et al. 2004, A&A, 415, L21

Chandrasekhar, S. 1950, Radiative Transfer (Oxford: Oxford Univ. Press)

Dlugach, J. M., Mishchenko, M. I., Liu, L., & Mackowski, D. W. 2011, J. Quant. Spectrosc. Radiat. Transfer, 112, 2068

Ermutlu, M., Muinonen, K., Lumme, K., Lindell, I., & Sihvola, A. 1995, J. Opt. Soc. Am. A, 12, 1310

Hapke, B. W., Nelson, R. M., & Smythe, W. D. 1993, Science, 260, 50

Lindell, I. V., Sihvola, A. H., Muinonen, K. O., & Barber, P. W. 1991, J. Opt. Soc. Am. A, 8, 472

Lommel, E. 1887, Acad. Wissensch. München, 17, 95

Lumme, K., & Penttilä, A. 2011, J. Quant. Spectrosc. Radiat. Transfer, 112, 1658

Mackowski, D. W. 2006, J. Quant. Spectrosc. Radiat. Transfer, 100, 237

Mackowski, D. W., & Mishchenko, M. I. 1996, J. Opt. Soc. Am. A, 13, 2266

Mackowski, D. W., & Mishchenko, M. I. 2011, J. Quant. Spectrosc. Radiat. Transfer, 112, 2182

Mishchenko, M. I. 1993, ApJ, 411, 351

Mishchenko, M. I. 2011, J. Quant. Spectrosc. Radiat. Transfer, 112, 2079

Mishchenko, M. I., & Dlugach, J. M. 1993, Planet. Space Sci., 41, 173

Mishchenko, M. I., Dlugach, J. M., & Liu, L. 2009a, Phys. Rev. A, 80, 053824

Mishchenko, M. I., Dlugach, J. M., Liu, L., et al. 2009b, ApJ, 705, L118

Mishchenko, M. I., & Liu, L. 2009, Appl. Opt., 48, 2421

Mishchenko, M. I., Liu, L., Mackowski, D. W., Cairns, B., & Videen, G. 2007, Opt. Express, 15, 2822

Mishchenko, M. I., Rosenbush, V. K., Kiselev, N. N., et al. 2010, Polarimetric Remote Sensing of Solar System Objects (Kyiv: Akademperiodyka), arXiv:1010.1171

Mishchenko, M. I., Travis, L. D., & Lacis, A. A. 2006, Multiple Scattering of Light by Particles (Cambridge: Cambridge Univ. Press)

Muinonen, K. 1989, in Proc. 1989 URSI Int. Symp. on Electromagnetic Theory Stockholm, 428

Muinonen, K. 1990, PhD dissertation, Univ. Helsinki
Muinonen, K. 2004, Waves Random Media, 14, 365
Muinonen, K., Piironen, J., Shkuratov, Yu. G., Ovcharenko, A., & Clark, B. E. 2002, in Asteroids III, ed. W. F. Bottke, Jr. et al. (Tucson, AZ: Univ. Arizona Press), 123
Muinonen, K., Sihvola, A., Lindell, I., & Lumme, K. 1991, J. Opt. Soc. Am. A, 8, 477
Muinonen, K., Tyynelä, J., Zubko, E., & Videen, G. 2010, Light Scattering Rev., 5, 477
Muinonen, K., & Videen, G. 2012, J. Quant. Spectrosc. Radiat. Transfer, 113, 2385
Muinonen, K., & Zubko, E. 2010, in Electromagnetic and Light Scattering XII, ed. d. K. Muinonen, A. Penttilä, H. Lindkvist, T. Nousiainen, & G. Videen (Helsinki: Helsinki Univ. Print), 194
Penttilä, A., & Lumme, K. 2011, J. Quant. Spectrosc. Radiat. Transfer, 112, 1741
Rosenbush, V., Kiselev, N., Avramchuk, V., & Mishchenko, M. 2002, in Optics of Cosmic Dust, ed. G. Videen & M. Kocifaj (Dordrecht: Kluwer), 191
Rosenbush, V. K., & Mishchenko, M. I. 2011, in Polarimetric Detection, Characterization, and Remote Sensing, ed. M. I. Mishchenko, Ya. S. Yatskiv, V. K. Rosenbush, & G. Videen (Dordrecht: Springer), 409
Saxon, D. S. 1955, Phys. Rev., 100, 1771
Shkuratov, Yu. G. 1988, Kinem. Fiz. Nebes. Tel, 4, 33
Shkuratov, Yu. G. 1989, Astron. Vestnik, 23, 176
Shkuratov, Yu. G., Muinonen, K., Bowell, E., et al. 1994, Earth Moon Planets, 65, 201
Stratton, J. A. 1941, Electromagnetic Theory (New York: McGraw-Hill)
Videen, G., & Kocifaj, M. (ed.) 2002, Optics of Cosmic Dust (Dordrecht: Kluwer)
Videen, G., Yatskiv, Ya., & Mishchenko, M. (ed.) 2004, Photopolarimetry in Remote Sensing (Dordrecht: Kluwer)
Voit, F., Schäfer, J., & Kienle, A. 2009, Opt. Lett., 34, 2593
Watson, K. M. 1969, J. Math. Phys., 10, 688
Zubko, E., Shkuratov, Yu., Mishchenko, M., & Videen, G. 2008, J. Quant. Spectrosc. Radiat. Transfer, 109, 2195